



This is a repository copy of *Electron irradiation induced nanocrystal formation in Cu-borosilicate glass*.

White Rose Research Online URL for this paper:  
<http://eprints.whiterose.ac.uk/100944/>

Version: Accepted Version

---

**Article:**

Sabri, M.M. and Moebus, G. (2016) Electron irradiation induced nanocrystal formation in Cu-borosilicate glass. *Journal of Nanoparticle Research*, 18 (3). 73. ISSN 1388-0764

<https://doi.org/10.1007/s11051-016-3376-3>

---

**Reuse**

Unless indicated otherwise, fulltext items are protected by copyright with all rights reserved. The copyright exception in section 29 of the Copyright, Designs and Patents Act 1988 allows the making of a single copy solely for the purpose of non-commercial research or private study within the limits of fair dealing. The publisher or other rights-holder may allow further reproduction and re-use of this version - refer to the White Rose Research Online record for this item. Where records identify the publisher as the copyright holder, users can verify any specific terms of use on the publisher's website.

**Takedown**

If you consider content in White Rose Research Online to be in breach of UK law, please notify us by emailing [eprints@whiterose.ac.uk](mailto:eprints@whiterose.ac.uk) including the URL of the record and the reason for the withdrawal request.



[eprints@whiterose.ac.uk](mailto:eprints@whiterose.ac.uk)  
<https://eprints.whiterose.ac.uk/>

# 1 **Electron irradiation induced nanocrystal formation in Cu-borosilicate glass**

2 Mohammed Mohammed Sabri . Günter Möbus

3 Department of Materials Science and Engineering, University of Sheffield, Sheffield S1 3JD, United Kingdom

4 e-mail: g.moebus@sheffield.ac.uk

## 5 **Abstract**

6 Nanoscale writing of Cu-nanoparticles in glasses is introduced using transmission electron  
7 microscopy (TEM) focused irradiation. Two types of copper borosilicate glasses, one with  
8 high and one with low Cu-loading, have been tested at energies of 200 - 300 keV and  
9 formation of Cu nanoparticles in a variety of shapes and sizes using different irradiation  
10 conditions is achieved. Electron energy loss spectroscopy (EELS) analysis, combined with  
11 high resolution transmission electron microscopy (HRTEM) imaging confirmed the  
12 irradiation-induced precipitated nanoparticles as metallic, while furnace annealing of the  
13 glass triggered dendrite-shaped particles of copper oxide. Unusual patterns of nanoparticle  
14 rings and chains under focused electron beam irradiation are also presented. Conclusively,  
15 electron beam patterning of Cu-loaded glasses is a promising alternative route to well  
16 established femtosecond-laser photoreduction of Cu-ions in glass.

17 **Keywords:** Borosilicate glass . Cu nanoparticles . Electron irradiation

18

## 19 **Introduction**

20 Studying the effects of electron irradiation in oxide glasses is a research field with long-  
21 standing track record but also recent interest (Sun et al. 2005; Bae et al. 2007; Sun et al.  
22 2004; Jiang and Silcox 2002; Meldrum et al. 1997; Sabri et al. 2015; Ollier et al. 2006;  
23 Möbus et al. 2008 ; Möbus et al. 2010). Electron beams induce various modifications in  
24 structure, composition and properties of the glass, such as phase separation and alkali  
25 migration (Sun et al. 2004; Jiang and Silcox 2002), precipitation (Meldrum et al. 1997; Sabri

1 et al. 2015), bubble formation (Ollier et al. 2006), fluidity enhancement and shape rounding  
2 (Möbus et al. 2008 ; Möbus et al. 2010).

3 Of particular interest is the irradiation induced generation of metal nanoparticles in glass.  
4 Nanoscale metal particles are known to exhibit physical and chemical properties, which are  
5 very different from the bulk materials (Wang et al. 2005). Copper nanoparticles together with  
6 other noble metals such as silver and gold are the most studied metallic nanoparticles. This is  
7 due to the fact that the surface plasmon resonances (SPR) feature in the optical spectra in the  
8 visible region (Yeshchenko et al. 2007). However, in comparison with Au and Ag, copper has  
9 the advantage of being low-cost and highly abundant while showing high conductivity.

10 Due to the high flexibility and high homogeneity of glasses they are considered to be an  
11 excellent host matrix to add different species. Copper nanoparticles embedded in silicate  
12 glasses are extremely promising materials for optical applications (Zhong et al. 2012; Teng et  
13 al. 2011) showing nonlinear optical properties (Almeida et al. 2012). The methods reported  
14 so far to precipitate copper in glass include for example ion implantation (Wang et al. 2010),  
15 femtosecond laser irradiation (Teng et al. 2010) and sol-gel followed by reduction and then  
16 nanoparticles growth via annealing (Zhong et al. 2013). Other metal nanoparticles have been  
17 generated by electron irradiation in glass as well (Jiang 2010; Singh and Karmakar 2011).

18 Cu in silica has been studied by Ito *et al* (Ito et al. 1999) who reported enlargement of pre-  
19 existing metallic copper nanoparticles in an amorphous SiO<sub>2</sub> film in scanning transmission  
20 electron microscopy. Outside the field of oxide glasses, electron beam irradiation-induced  
21 formation of copper nanoparticles of various diameters in different materials has been  
22 reported (Pham et al. 2011; Yen et al. 2004; Zhou et al. 2008).

23 Up to date, however, no research is known in electron irradiation-induced precipitation of Cu  
24 nanocrystals in glasses. Therefore, in the present paper we report on the *in-situ* formation of

1 copper nanoparticles in glass using the impact of electron beam irradiation in transmission  
2 electron microscopy with prospects of achieving high-resolution beam control and patterning  
3 capabilities in the future.

#### 4 **Experimental details**

##### 5 Glass composition and melting process

6 The compositions of the main oxide glasses used in this study and given acronyms of  
7 CuNBS-A and CuNBS-B across the paper are  $20\text{CuO}-15\text{Na}_2\text{O}-15\text{B}_2\text{O}_3-50\text{SiO}_2$  and  $1\text{CuO}-$   
8  $15\text{Na}_2\text{O}-15\text{B}_2\text{O}_3-69\text{SiO}_2$  (in mol.%), respectively. The motivation for the choice of the  
9 compositions is to explore a concentration range of Cu which is either as low as frequently  
10 used in laser-patterning of various Cu-silicate glasses (Almeida et al. 2012; Teng et al. 2010),  
11 or as high as to provide compatibility with some of our earlier and ongoing work on other  
12 alkali-borosilicate glasses (e.g. loaded with Zn, Ag and others, as reported elsewhere (Sabri et  
13 al. 2015; Yang et al. 2006; Yang et al. 2006)). Both Cu concentrations are low enough to fall  
14 inside the glass forming region of the underlying ternary N-B-S phase diagram. The glass  
15 batch has been prepared by mixing powders of copper oxide (CuO, purity > 99%), boric acid  
16 ( $\text{H}_3\text{BO}_3$ , purity > 99.5%), sodium carbonate ( $\text{Na}_2\text{CO}_3$ , purity ~ 99.1%) and silica sand ( $\text{SiO}_2$ ,  
17 purity ~ 99.5%) to obtain 200 g glass melt. After melting in a mullite crucible and electric  
18 furnace at  $1400^\circ\text{C}$  about 80% of the melt is poured into a pre-heated stainless steel mould  
19 while 20% is rapidly cooled by pouring into water to obtain a glass frit. The glass block was  
20 annealed at  $550^\circ\text{C}$  with return to room temperature at  $1^\circ\text{C}/\text{min}$ .

##### 21 Sample preparation for electron microscopy

22 The glass frit was exclusively examined by TEM: specimens were prepared by grinding the  
23 quenched glass frit into a very fine powder in acetone using a pestle and mortar. After ultra-  
24 sonication for about 15 min the powder was placed on a holey carbon film, here supported by

1 a gold grid, instead of the usual copper grid, such as to avoid overlap of copper EDX signals  
2 from the glass and from the grid. The annealed glass was examined by x-ray diffraction  
3 (XRD) and both TEM and SEM. Initially the glass block is cut twice in cross section by a  
4 diamond cutting saw into a thin slice of about 2×2 cm cross section. For SEM this slice is  
5 then ground using various grit wheels and polished by a diamond paste and carbon coated  
6 against charging. For TEM and XRD, only grinding was used, making sure that the outer  
7 regions of the cross-sectional slice are cut off and excluded, as they might be less typical due  
8 to their faster cooling rate in contact with air or the metal mould.

#### 9 Electron irradiation and imaging process

10 In this research, TEMs of type JEOL JEM 2010F field emission gun (FEG) and JEOL JEM  
11 3010 LaB<sub>6</sub> thermal filament operating at 200 and 300 keV respectively have been used for  
12 the purpose of both imaging (low intensity) and deliberate electron beam (high intensity)  
13 irradiation. Electron energy loss spectroscopy (EELS) and energy dispersive x-ray (EDX)  
14 spectroscopy are used on the JEOL JEM 2010F. On both TEMs, most of the irradiation is  
15 applied with largest condenser aperture (CA) and spot size 1. Irradiation densities range from  
16 0.01 pA/ nm<sup>2</sup> for low-intensity imaging over <1 pA nm<sup>2</sup> for our chosen "standard" converged  
17 irradiation conditions and >3 pA/ nm<sup>2</sup> for special high-current conditions with condenser  
18 aperture removed. On the other hand, SEM images (both secondary electron (SE) and  
19 backscattered electron (BSE)) were taken using FEI Inspect F, selected at 20 kV, also  
20 equipped with EDX.

21

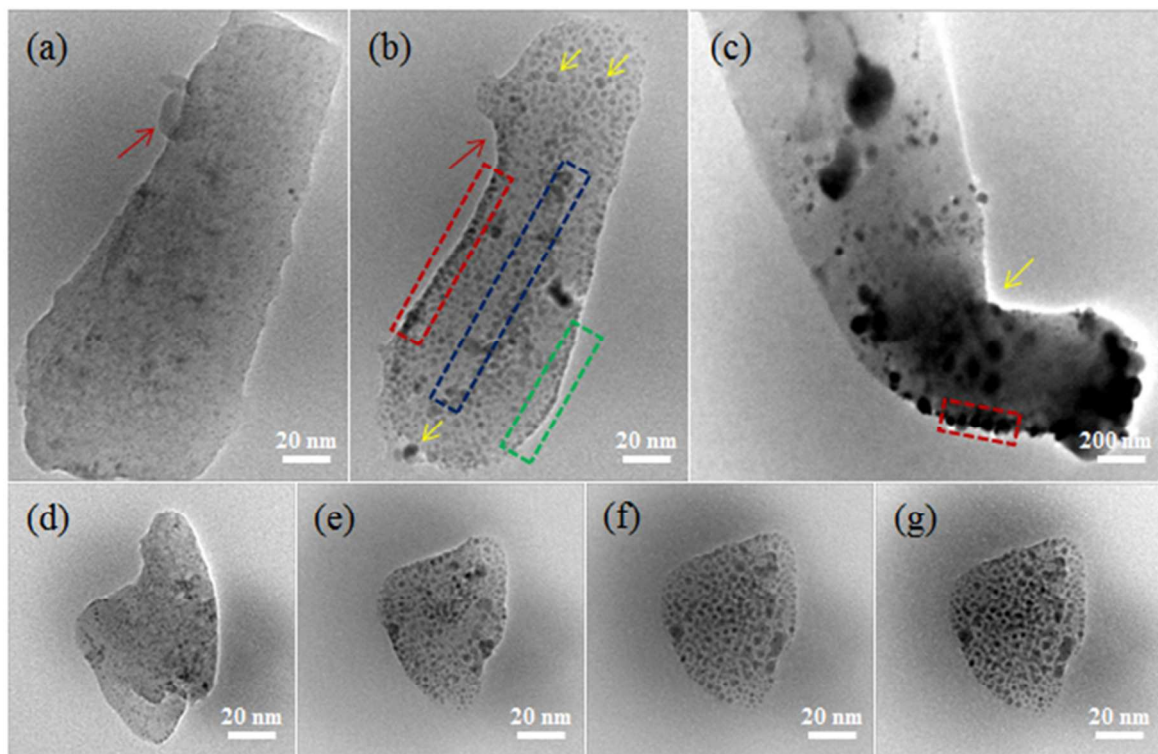
22

23

# 1 Results

## 2 TEM irradiation and imaging of quenched glass

3 Three rod shaped frit CuNBS-A glass fragments were selected for different electron  
4 irradiation conditions (Fig. 1). The top row is meant to study dose variation via changes of  
5 beam current, while the bottom row contains dose variation via exposure at constant current.



6

7 **Fig. 1** TEM micrographs of frit CuNBS-A glass fragments; JEM TEM 3010 at 300 keV.

8 (a-c): Intensity series; (a) imaging radiation only; (b) after about 3 min of standard convergent  
9 electron beam irradiation. (c) similar glass fragment after irradiation with open-aperture (high  
10 current) for about 2 min. (d-g) Time series at constant intensity (standard convergent beam,  
11 aperture inserted), including intervals of 3 minutes added irradiation between each image.

12

13 At the first stage, see Fig. 1a, using weak wide-beam (full screen) imaging illumination the  
14 initial glass fragment of roughly 60 nm × 250 nm size is rather homogeneous, except for

1 some speckle. Upon comparison with the surrounding amorphous carbon-film, some  
2 coherency-speckle existing for all amorphous materials in HRTEM can be observed (focus-  
3 dependent), and in addition we identify a small number of true clusters or precipitates, which  
4 are darker and sharper (<3 nm-sized). We believe these fine Cu clusters and small particles  
5 have formed during the early stages of focusing and preparing the electron beam for  
6 irradiation. Subsequently, the main precipitation experiment was triggered by systematic  
7 electron beam convergence to a diameter slightly larger than 200 nm for about 3 min  
8 irradiating the entire glass fragment. Fresh nanoparticles of isotropic morphologies  
9 precipitated through the entire glass fragment. The distribution of these nanoparticles is rather  
10 homogeneous and diameters range from about 1-12 nm (yellow arrows for largest NPs in Fig.  
11 1b). These particles have grown by extraction of Cu from the glass, with the matrix getting  
12 brighter (more transparent) and include enlargements of any pre-existing clusters from Fig.  
13 1a, but most of them are newly nucleated particles. As a side effect, some smoothing of rough  
14 surfaces of the glass fragment and rounding-off of the glass corners (Möbus et al. 2010) is  
15 observed, also including the merging (fusion/welding) of the main glass with an originally  
16 separate attached glass particle (red arrow on Fig. 1a,b). An overall shrinkage of the volume  
17 of the glass fragment indicating some ablation of the Na-B-Si-oxide network is found.  
18 Remarkably, formation of particle chains in the glass fragment is evident with the first chain  
19 being about 90 nm long and consisting of about 23 nanoparticles (indicated by red dashed  
20 area in Fig. 1b), while the opposite second chain (green dashed area in Fig. 1b) is shorter.  
21 Both are just inside the edge of the glass fragment along its long aspect. A third chain of  
22 nanoparticles can be seen in the centre of the glass fragment, again parallel to the long axis  
23 (blue dashed area in Fig. 1b), and this consists of a mixture of small and few large  
24 nanoparticles. Due to the large particle numbers involved in these very systematic chains,  
25 they are true 3D chains and cannot be a projection artefact (Xu et al. 2008). The 3<sup>rd</sup> stage of

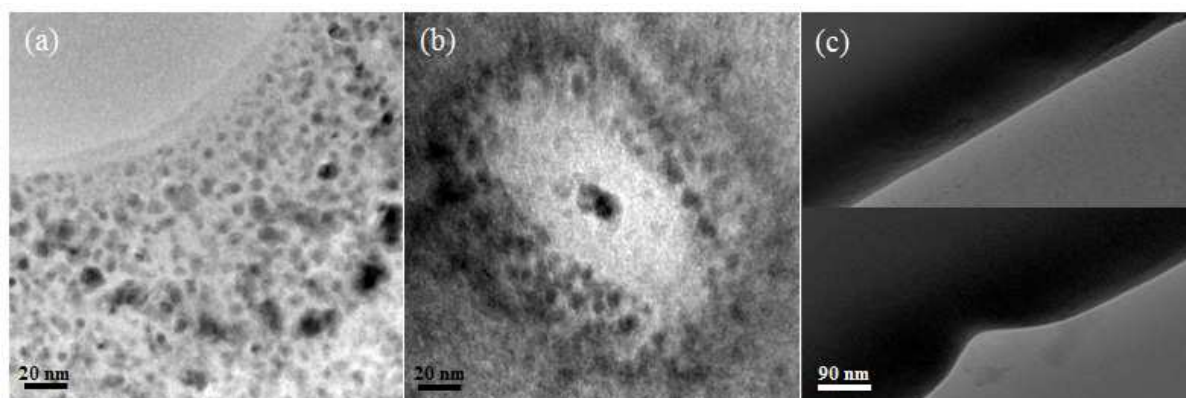
1 the intensity-series involves irradiation of another glass rod-fragment (initially looking  
2 similar to Fig. 1a) via removing the condenser aperture, increasing currents by a factor 11.  
3 After ~ 2 min of electron irradiation, fewer and larger nanoparticles are formed with less  
4 circular shapes distributed very in-homogeneously through the glass rod. This indicates a  
5 growth and ripening stage, merging multiple particles, with no more Cu extracted from the  
6 glass. The residual glass matrix in regions of >200 nm is now very bright and transparent,  
7 virtually Cu-free and speckle-free. Several small nanoparticles are also stacked outside the  
8 glass rod touching its edges and some others of diameter of about 50 nm are found in an  
9 ordered state outside the glass rod, near the edge, denoted by the red dashed area in Fig. 1c.  
10 The glass rod bending (yellow arrow) of the originally straight rod is another irradiation  
11 result.

12 Complementary, the exposure-time series at constant current (Fig. 1d-g) reveals formation of  
13 clusters and small round particles over multiple applications of 3 min additional irradiation.  
14 This series started with pre-irradiation levels triggering cluster formation already in Fig. 1d,  
15 however, after switching to the higher current for Fig. 1e, the small particles of Fig. 1d are  
16 not traceable to grow, but rather replaced by mostly new and larger particles. This coincides  
17 with a fragment-change morphing the glass into a more roundish shape. However, the  
18 precipitation saturates quickly in Fig. 1f,g and no ripening occurs unlike in Fig 1c, indicating  
19 lack of long-range diffusion, and therefore lack of temperature.

20 To reveal further aspects about radiation induced precipitation mechanisms, we now switch  
21 from homogeneous illumination of an entire glass fragment to local electron beam irradiation,  
22 with beam diameter much smaller than the fragment. In such situations, beam-induced ring  
23 formation has been previously reported in silicate glasses (Jiang et al. 2003) but not so far  
24 involving copper. Figure 2a,b shows the impact of irradiation in a FEG-TEM, with beam



1 focused to 100-150 nm, showing the formation of nanoring-like structures of nanoparticles in  
2 the frit CuNBS-A glass.

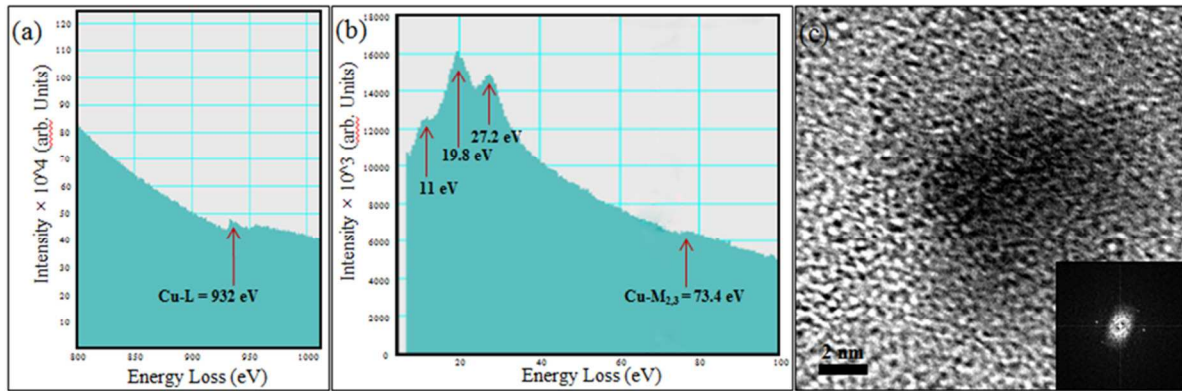


3  
4 **Fig. 2.** (a,b) Formation of ring-like Cu nanoparticles in the glass fragment of frit CuNBS-A  
5 using focused electron beam in JEM TEM 2010F at 200 keV. (c) CuNBS-B glass before  
6 (upper) and after (lower) 6 min of electron irradiation in JEM TEM 3010 at 300 keV.

7  
8 In Fig. 2a, a medium intense electron beam of diameter of about 140 nm for about 5 min  
9 irradiation generated nanoparticles of 8-15 nm size along the ring and smaller sub-10 nm NPs  
10 inside the ring. Nearby irradiation with more focused electron beam in a thicker glass  
11 fragment area (Fig. 2b) generated a dark ring with one central dark particle separated by  
12 significantly lighter areas due to Cu-depletion and/or glass matrix ablation. To compare the  
13 response of high and low Cu loaded glasses (CuNBS-A versus CuNBS-B), Figure 2c shows a  
14 glass rod of CuNBS-B being irradiated on its edge for about 6 min. No Cu nanoparticles or  
15 clusters are visible at the region under irradiation, while significant glass ablation is obvious.

16 An EELS spectrum from the region of irradiation of glass CuNBS-A in Fig. 2a is shown in  
17 Fig. 3a.

18



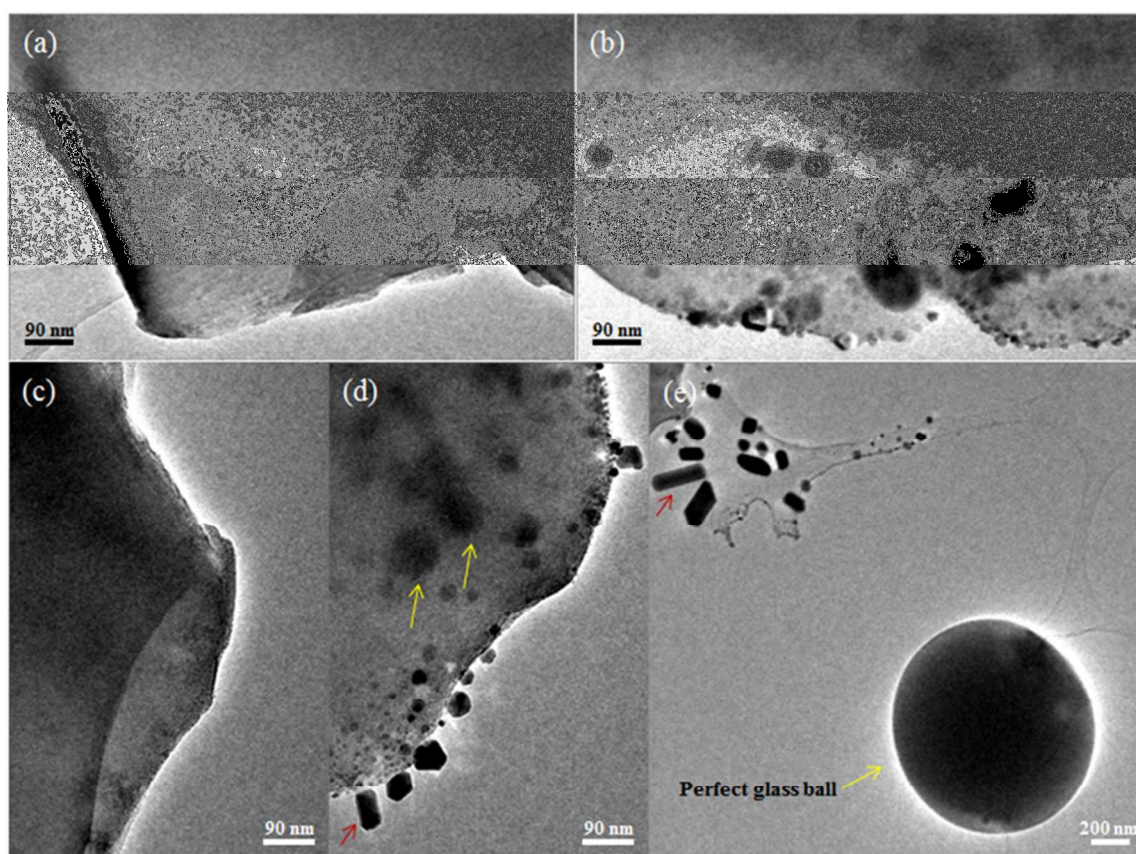
1

2 **Fig. 3.** EELS spectra of frit CuNBS-A glass fragments after irradiation showing (a) L-edge  
 3 for particle in glass, (b) low loss spectrum showing plasmon-range peaks and  $M_{2,3}$  edge for  
 4 metal particle, (c) HRTEM image for a typical nanoparticle in glass with FFT as inset.

5

6 The main peak appearing in the EEL spectrum at around 932 eV with an onset around 929 eV  
 7 (Fig. 3a) becomes very distinct after few minutes of irradiation, corresponding to the Cu-L  
 8 edge (within expected calibration uncertainties), due to the glass matrix thinning while Cu  
 9 segregation pushing Cu-concentration locally. Comparing literature data for fine structure  
 10 between Cu, CuO and Cu<sub>2</sub>O (Ito et al. 1999; Long and Petford-Long 1986; Yang et al. 2014),  
 11 the shape of the L-edge of Fig. 3a clearly matches metallic copper, as oxides would show two  
 12 high-contrast "white lines". Complementary, Fig. 3b shows a low loss EEL spectrum acquired  
 13 on one particle as of Fig. 4e, and the peak with onset around 73.4 eV matches the  $M_{2,3}$  edge,  
 14 although not distinctive between metal and oxides (Ahn et al. 1983). However, two  
 15 distinguishing peaks at around 19.8 and 27.2 eV respectively well match metallic copper  
 16 (Ahn et al. 1983), as oxide would show a single broad peak around 22 eV. Together with the  
 17 small peak at around 11 eV all those three peaks match literature data (computer modelling  
 18 and earlier experiments) for metallic copper, while the origin of these "plasmon-range" peaks  
 19 has been attributed to d-band interband transitions in (Hébert et al. 2011).

1 For further confirmation, Fig. 3c shows HRTEM of a typical precipitate NP from the  
2 irradiation region in Fig. 2a with fast Fourier transformation (FFT) as inset, from which a d-  
3 spacing can be extracted compatible with metallic copper.  
4 It is worthwhile to expand our observations to cases where segregated and expelled Cu does  
5 not precipitate inside the glass only but deposits on the glass fragment surface or even in its  
6 vicinity of the support film as shown in Fig. 4.



7  
8 **Fig. 4.** Surface decoration with Cu using frit CuNBS-A glass; JEM TEM 3010 at 300 keV.  
9 (a) completely cluster and particle-free pristine glass; (b) after 2 min irradiation; (c-e): 2<sup>nd</sup>  
10 glass fragment series consists of (c) zero and (d) 2 min standard irradiation, while (e) shows  
11 delocalised formation of Cu nanocrystals on nearby C-film and sudden transformation of a  
12 glass fragment into a perfect glass ball under open-aperture high level of irradiation.

13

1 The initial views of the two glass fragments (Fig. 4a,c) are important examples where pre-  
2 irradiation was successfully minimised, such that no clusters or particles are visible at all. The  
3 speckle in the fragment is of same level than in the neighbouring carbon film, and therefore  
4 confirms coherency-speckle typical for amorphous materials while no sharp and black  
5 particles, indicating Cu, are visible. Irradiation experiments in Fig. 4b (condenser aperture  
6 inserted) and Fig. 4d (no condenser aperture), resulted in the formation of surface-deposited  
7 NPs, clearly outside the original glass perimeter. Particularly well-faceted morphology and  
8 shapes, typical of single crystal of metallic Cu, are seen in Fig. 4d. Contrary, roundish-shape  
9 NPs are still formed inside the original glass with diameter of about 5-35 nm, except for two  
10 large NPs of  $\sim 77$  nm (yellow arrows in Fig. 4d). A large surface crystal is marked by red  
11 arrow. Another irradiation of a nearby glass fragment with condenser aperture removed  
12 resulted in formation of large-distance evaporated well-faceted Cu nanocrystals of which the  
13 largest has dimensions of about  $260 \text{ nm} \times 64 \text{ nm}$  (red arrow in Fig. 4e), sitting  $> 1 \mu\text{m}$  away  
14 from the original glass fragment which itself became transformed into a perfect ball (Möbus  
15 et al. 2010) of diameter of  $\sim 1 \mu\text{m}$  (Fig. 4e). We believe that the sequence of these  
16 phenomena is, (i) firstly electron irradiation-induced precipitation of metallic Cu, (ii)  
17 followed by electron beam ablation of both Cu and glass matrix with re-deposition of metallic  
18 copper onto the carbon film away from the original glass fragment, (iii) and finally  
19 transformation of the residual not yet ablated glass fragment into a perfect ball due to surface  
20 tension.

21

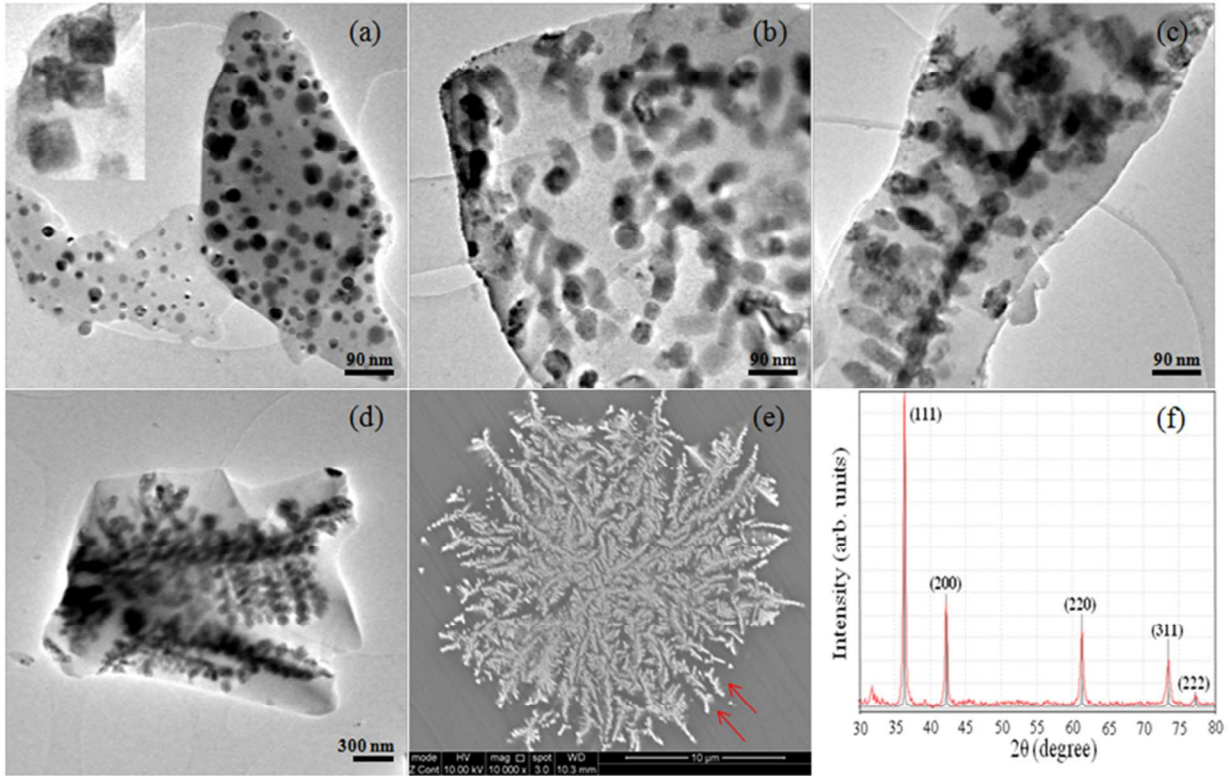
22

23

24

25

- 1 TEM and SEM imaging of annealed CuNBS-A glass
- 2 The annealed version of CuNBS-A glass has been investigated in Fig. 5.



3  
 4 **Fig. 5.** (a-d) TEM (JEM TEM 3010 at 300 keV) images of annealed CuNBS-A glass  
 5 spherical (a), square (the inset in (a)) and dendritic (b-d) shape of Cu<sub>2</sub>O precipitates. (e) SEM  
 6 image of a typical dendrite copper oxide particle. (f) XRD pattern of annealed CuNBS-A  
 7 glass.

8 The precipitated nano/micro-particles, of dendrite-like shapes, are sorted by the degree of  
 9 completeness of dendrite development from Figs. 5a towards 5e. The existence of various  
 10 shapes, starting from spherical (Fig. 5a) and square (Fig. 5a, inset) particles up to well-  
 11 developed dendrite branching systems, is due to different thermal history and temperature  
 12 gradient. While we avoided inclusion of surface-near material by cutting it off, the remaining  
 13 inner glass would still have experienced a cooling speed gradient as a radial function from the  
 14 centre distance. The TEM images are believed to be fragments of larger dendrites, seen on

1 the microscale via SEM imaging (Fig. 5e). An XRD pattern of CuNBS-A glass is shown in  
2 Fig. 5f. Dominant peaks at  $2\theta = 36.4^\circ$  ( $d=2.466 \text{ \AA}$ ),  $2\theta = 42.3^\circ$  ( $d=2.135 \text{ \AA}$ ),  $2\theta = 61.34^\circ$   
3 ( $d=1.510 \text{ \AA}$ ) and  $2\theta = 73.5^\circ$  ( $d=1.287 \text{ \AA}$ ) correspond to the planes of (111), (200), (220) and  
4 (311) of the cubic  $\text{Cu}_2\text{O}$  phase, respectively, along with a relatively weak peak at  $2\theta = 77.3^\circ$   
5 ( $d=1.233 \text{ \AA}$ ) corresponding to (222). SEM-EDX analysis (not shown here) reveals copper  
6 oxide signals overlapping the glass matrix, while also a small Al peak shows, which is  
7 believed to be a residue from the crucible used in glass melting. The overall length of the  
8 dendrite is about  $20 \mu\text{m}$  with few  $\mu\text{m}$  long sub-branches indicated by red arrows. The  
9 dendrites with central backbone and multi-branch structures (Fig. 5b & 5c) are consistent  
10 with Kumaran *et al* (Kumaran et al. 2013). The fact that in Fig. 5c,d the dendrite is preserved  
11 in the centre of the fragment with its backbone oriented parallel to the fracture surface during  
12 grinding indicates mechanical toughening of the glass composite material by the Cu-  
13 dendrites.

14

## 15 **Discussions**

16 The formation of Cu particles through electron beam irradiation seems to follow an intensity-  
17 dose dependent schedule: (i) initially very fine particles are nucleated at widely dispersed  
18 locations, sometimes even at the low intensity imaging irradiation (Fig. 1a, 1d), but this  
19 premature precipitation could be suppressed in the examples of Fig. 4a and 4c. (ii)  
20 Irradiation under standard converged beam conditions subsequently leads to further  
21 nucleation and growth of particles up to 10 nm-size range, achieved homogeneously filling  
22 the entire glass volume, with the glass matrix getting paler indicating that Cu still segregates  
23 from glass, not from other clusters. This stage is the saturated end-stage for middle intensity  
24 levels and increasing dose via time does not alter the structure, as obviously the diffusion  
25 constants for long-range diffusion necessary for Ostwald ripening are too low. (iii) Only at

1 extreme intensities, with open apertures, large Cu-particles grow by ripening on the cost of  
2 smaller ones, leaving Cu-free space in between, with the large diffusion distances covered by  
3 Cu atoms pointing to beam-induced heating in addition to radiation-induced fluidity (RIF).  
4 As for surface decoration, Fig. 4, we propose that the faceted metallic Cu, surface-bound or  
5 found on the C-film, is a secondary synthesis effect upon irradiation of metallic Cu initially  
6 formed at (but still within) the glass surface, as reported for Ag in (Li and Zhang 2010) and  
7 for Co and Ni in halides in (Gnanavel and Möbus 2012). The fact that those particles form on  
8 opposite ends of C-film holes favours a kind of "thermal evaporation" deposition, rather than  
9 an atomic diffusion on the C-film itself. For the low-Cu glass (CuNBS-B) irradiation had not  
10 triggered any visible precipitation even at levels of intensity high enough to ablate the entire  
11 glass matrix. Possibly, combination of irradiation and heat treatment (which would require a  
12 TEM heating holder) would have achieved particle formation, similarly to laser induced  
13 nucleation with subsequent heat treatment (Almeida et al. 2012) for particles. Apart from  
14 observing ring formations, also centre positions in impact craters (Fig. 2b) or centre positions  
15 in rods (Fig. 1b) seem to be areas of stationary Cu location as any (e.g. electrostatic) driving  
16 force there to move these cations to the edge of glass fragment or to the edge of the beam  
17 impact area would cancel.

18 The purpose for including our comparative study of annealed glass fragments is to elucidate  
19 the need for suppression of thermal precipitation, confirming that a cooling-rate at least as  
20 fast as in our frit-quenching is mandatory. Indeed, further beam irradiation of the fragments  
21 in Fig. 5 did not lead to any new particles or changes to existing dendrites. The reasons why  
22 thermal annealing produces  $\text{Cu}_2\text{O}$  while "electron beam annealing" produces metallic Cu, is  
23 due to the redox environment, as we used air-furnace heating for annealing, while the TEM-  
24 exposure is a reducing medium.

25

## 1 **Conclusions**

2 We have demonstrated that nm-controllable electron beams can be used, complementary to  
3 the well-established laser irradiation researches, to precipitate nm-sized Cu-particles from a  
4 glass-matrix. This will be of interest for application areas ranging from glass-index grading,  
5 reflectivity engineering and wave-guiding, over surface-plasmon coupling of light or other  
6 nanoplasmonics, onto information storage and radiation-recording strategies, or most widely  
7 the modulation and modification of glass-surface appearance for visual or mechanical  
8 property tuning. Our method of open condenser aperture irradiation in TEM allowed *in-situ*  
9 observation of processes otherwise only known from thermal annealing, or from high-power  
10 electron beam instruments (e.g. welders or EPMA). Forthcoming work will extend our above  
11 results into systematic pattern generation via nm-localised automatic beam positioning and  
12 movement control.

13

## 14 **Acknowledgments**

15 We thank the Iraqi Kurdistan Regional Government/Ministry of Higher Education and  
16 Scientific Research for the funding of the project as a part of Human Capacity Development  
17 Program (HCDP). The authors also thank Professor Russell J Hand for his helpful  
18 contribution.

19

## 20 **References**

- 21 Ahn CC, Krivanek OL, Burgner RP, Disko MM, Swann PR (1983) Electron energy loss  
22 spectroscopy Atlas. ASU HREM Facility and Gatan, Inc  
23  
24 Almeida JMP, De Boni L, Avansi W, Ribeiro C, Longo E, Hernandez AC, Mendonca CR  
25 (2012) Generation of copper nanoparticles induced by fs-laser irradiation in borosilicate  
26 glass. Opt. Exp 20:15106-15113  
27  
28 Bae IT, Zhang Y, Weber WJ, Higuchi M, Giannuzzi LA (2007) Electron-beam induced  
29 recrystallization in amorphous apatite. Appl. Phys. Lett 90:021912  
30  
31 Gnanavel T, Möbus G (2012) In situ synthesis of cobalt nanocrystal hierarchies in a  
32 transmission electron microscope. J. Nanopart. Res 14:683-694



- 1 Hébert C, Alkauskas A, Löffler S, Jouffrey B, Schattschneider P (2011) Capturing EELS in  
2 the reciprocal space. *Eur. Phys. J. Appl. Phys* 54:33510  
3
- 4 Ito Y, Jain H, Williams DB (1999) Electron-beam induced growth of Cu nanoparticles in  
5 silica glass matrix. *Appl. Phys. Lett* 75:3793-3795  
6
- 7 Jiang N (2010) Electron-beam fabrication of nanostructures in glasses *Microsc. Microanal*  
8 16:1660-1661  
9
- 10 Jiang N, Hembree GG, Spence JCH, Qiu J, Garcia de Abajo FJ, Silcox J (2003) Nanoring  
11 formation by direct-write inorganic electron-beam lithography. *Appl. Phys. Lett* 83:551-553  
12
- 13 Jiang N, Silcox J (2002) Electron irradiation induced phase decomposition in alkaline earth  
14 multi-component oxide glass. *J. Appl. Phys* 92:2310-2316  
15
- 16 Kumaran CKS, Agilan S, Velauthapillai D, Muthukumarasamy N, Thambidurai M,  
17 Balasundaraprabhu R, Senthil TS (2013) Preparation and characterization of copper dendrite  
18 like structure by chemical method. *Adv. Mater. Res* 678:27-31  
19
- 20 Li K, Zhang FS (2010) Novel approach for preparing silver nanoparticles under electron  
21 beam irradiation. *J. Nanopart. Res* 12:1423-1428  
22
- 23 Long NJ, Petford-Long AK (1986) In-situ electron-beam-induced reduction of CuO: A study  
24 of phase transformations in cupric oxide. *Ultramicroscopy* 20:151-159  
25
- 26 Meldrum A, Boatner LA, Ewing RC (1997) Electron-irradiation-induced nucleation and  
27 growth in amorphous LaPO<sub>4</sub>, ScPO<sub>4</sub>, and zircon. *J. Mater. Res* 12:1816-1827  
28
- 29 Möbus G, Ojovan M, Cook S, Tsai J, Yang G (2010) Nano-scale quasi-melting of alkali-  
30 borosilicate glasses under electron irradiation. *J. Nucl. Mater.* 396:264-271
- 31 Möbus G, Tsai J, Xu XJ, Bingham P, Yang G (2008) Nanobead formation and  
32 nanopatterning in glasses. *Microsc. Microanal* 14:434-435  
33
- 34 Ollier N, Rizza G, Boizot B, Petite G (2006) Effects of temperature and flux on oxygen  
35 bubble formation in Li borosilicate glass under electron beam irradiation *J. Appl. Phys.*  
36 99:073511
- 37 Pham LQ, Sohn JH, Park JH, Kang HS, Lee BC, Kang YS (2011) Comparative study on the  
38 preparation of conductive copper pastes with copper nanoparticles prepared by electron beam  
39 irradiation and chemical reduction. *Radia. Phys. Chem* 80:638-642  
40
- 41 Sabri MM, Hand RJ, Möbus G (2015) Zn nanodot patterning in borosilicate glasses by  
42 electron irradiation. *J. Mater. Res* 30:1914-1924  
43
- 44 Singh SP, Karmakar B (2011) In situ electron beam irradiated rapid growth of bismuth  
45 nanoparticles in bismuth-based glass dielectric at room temperature. *J. Nanopart Res*  
46 13:3599-3606  
47

- 1 Sun K, Wang LM, Ewing RC, Weber WJ (2004) Electron irradiation induced phase  
2 separation in a sodium borosilicate glass. Nucl. Instrum. Methods Phys. Res. Sect. B  
3 218:368-374  
4
- 5 Sun K, Wang LM, Ewing RC, Weber WJ (2005) Effects of electron irradiation in nuclear  
6 waste glasses. Philos. Mag 85:597-608  
7
- 8 Teng Y, Qian B, Jiang N, Liu Y, Luo F, Ye S, Zhou J, Zhu B, Zeng H, Qiu J (2010) Light  
9 and heat driven precipitation of copper nanoparticles inside Cu<sup>2+</sup>-doped borate glasses.  
10 Chem. Phys. Lett 485:91-94
- 11 Teng Y, Zhou J, Luo F, Lin G, Qiu J (2011) Controllable space selective precipitation of  
12 copper nanoparticles in borosilicate glasses using ultrafast laser irradiation. J. Non-Cryst.  
13 Solids 357:2380-2383
- 14 Wang X, Zhuang J, Peng Q, Li Y (2005) A general strategy for nanocrystal synthesis. Nature  
15 431:121-124  
16
- 17 Wang YH, Wang YM, Lu JD, Ji LL, Zang RG, Wang RW (2010) Nonlinear optical  
18 properties of Cu nanoclusters by ion implantation in silicate glass. Opt. Commu 283:486-489
- 19 Xu X, Saghi Z, Yang G, Hand RJ, Möbus G (2008) Three-dimensional structure of CeO<sub>2</sub>  
20 Nanodendrites in Glass. Cryst. Growth Des 8:1102-1105  
21
- 22 Yang G, Cheng S, Li C, Zhong J, Ma C, Wang Z, Xiang W (2014) Investigation of the  
23 oxidation states of Cu additive in colored borosilicate glasses by electron energy loss  
24 spectroscopy. J. Appl. Phys 116:223707  
25
- 26 Yang G, Möbus G, Hand RJ (2006) Cerium and Boron Chemistry in Doped Borosilicate  
27 Glasses Examined by EELS. Micron 37:433-441  
28
- 29 Yang G, Möbus G, Hand RJ (2006) EELS Study of Boron Coordination in Alkali  
30 Borosilicate Glasses under Extensive Electron Irradiation. Phys. Chem. Glass 47:507-512  
31
- 32 Yen MY, Chiu CW, Chen FR, Kai JJ, Lee CY, Chiu HT (2004) Convergent electron beam  
33 induced growth of copper nanostructures: Evidence of the importance of soft template.  
34 Langmuir 20:279-281
- 35 Yeshchenko OA, Dmitruk IM, Dmytruk AM, Alexeenko AA (2007) Influence of annealing  
36 conditions on size and optical properties of copper nanoparticles embedded in silica matrix.  
37 Mater. Sci. Eng 137:247-254
- 38 Zhong J, Xiang W, Chen Z, Zhao H, Liang X (2013) Structural, Linear and third-order  
39 nonlinear optical properties of Cu nanocrystal in sodium borosilicate glass. Mater. Sci. Eng.  
40 B 178:998-1003  
41
- 42 Zhong J, Xiang W, Zhao H, Zhao W, Chen G, Liang X (2012) Synthesis, characterization,  
43 and third-order nonlinear optical properties of copper quantum dots embedded in sodium  
44 borosilicate glass. J. Alloys. Compd 537:269-274  
45

- 1 Zhou R, Wu X, Hao X, Zhou F, Li H, Rao W (2008) Influences of surfactants on the
- 2 preparation of copper nanoparticles by electron beam irradiation. Nucl. Instrum. Methods
- 3 Phys. Res. Sect. B 266:599-603
- 4